

# TF3P: Three-dimensional Force Fields Fingerprint Learned by Deep Capsular Network

Yanxing Wang<sup>†</sup>, Jianxing Hu<sup>†</sup>, Junyong Lai, Yibo Li, Hongwei Jin, Lihe Zhang, Liangren Zhang\*, Zhenming Liu\*

State Key Laboratory of Natural and Biomimetic Drugs, School of Pharmaceutical Sciences, Peking University, Beijing, 100191, P. R. China

Author Email Address:

Yanxing Wang: yh\_wang@bjmu.edu.cn;

Jianxing Hu: j.hu@pku.edu.cn;

Junyong Lai: jylai@bjmu.edu.cn;

Yibo Li: ybli@pku.edu.cn;

Hongwei Jin: jinhw@bjmu.edu.cn;

Lihe Zhang: zdszlh@bjmu.edu.cn;

Liangren Zhang: liangren@bjmu.edu.cn;

Zhenming Liu: zmliu@bjmu.edu.cn.

<sup>†</sup>: These authors contribute equally.

\*: To whom correspondence should be addressed.

## Abstract:

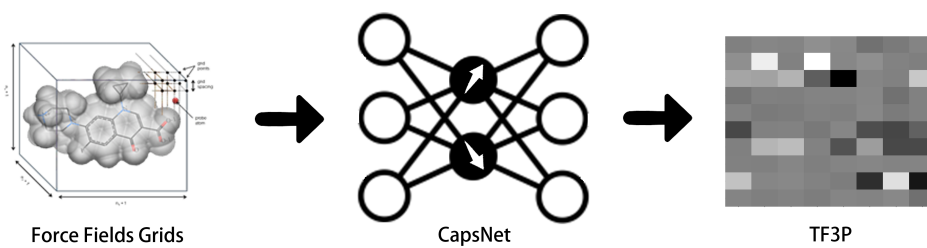
Molecular fingerprints are the workhorse in ligand-based drug discovery. In recent years, increasing number of research papers reported fascinating results on using deep neural networks to learn 2D molecular representations as fingerprints. One may anticipate that the integration of deep learning would also contribute to the prosperity of 3D fingerprints. Here, we presented a new 3D small molecule fingerprint, the three-dimensional force fields fingerprint (TF3P), learned by deep capsular network whose training is in no need of labeled dataset for specific predictive tasks. TF3P can encode the 3D force fields information of molecules and demonstrates its stronger ability to capture 3D structural changes, recognize molecules alike in 3D but not in 2D, and recognize similar targets inaccessible by other fingerprints, including the solely existing 3D fingerprint E3FP, based on only ligands similarity. Furthermore, TF3P is compatible with both statistical models (e.g. similarity ensemble approach) and machine learning models. Altogether, we report TF3P as a new 3D small molecule fingerprint with promising future in ligand-based drug discovery.

**Keywords:** Deep Learning; Molecular Fingerprint; Force Fields

## Highlights:

- A new 3D fingerprint, TF3P, was developed using deep capsular network without specific labeled data;
- TF3P is more sensitive to 3D structural changes than E3FP and able to recognize molecules alike in 3D but not in 2D;
- TF3P outperforms E3FP and 2D fingerprints on finding similar targets by similar ligands;
- TF3P is compatible with both statistical models and machine learning models.

## Graphic Abstract:



## Introduction

It’s a primary principle in ligand-based drug discovery that similar ligands bind to similar targets<sup>1</sup>. This statement in essence is to infer target similarity from only ligand information. Over the past decades of endeavor to improve this inference with more precision, molecular representation is a useful tool in cheminformatics<sup>2-5</sup> and can be divided into two categories intuitively, namely 2D and 3D representations.

Since the 1970s, 2D molecular fingerprints have developed maturely and can be classified into four types<sup>3</sup>, namely substructure fingerprints (e.g. MACCSKey<sup>6</sup>), circular fingerprints (e.g. ECFP<sup>7</sup>), topological fingerprints and pharmacophores. In addition to these classical molecular fingerprints designed by chemists, with the advent of deep learning in recent years, increasing number of research papers reported on using deep neural networks (DNN) to fingerprint 2D molecules<sup>8-13</sup>. Of particular note is Attentive FP<sup>12</sup> which can predict large, non-local conjugated aromatic systems from merely atomic features without bond features.

Compared to use 2D representation, using molecular 3D representation<sup>14</sup> is expected to enhance the performance of predictive models, especially in the prediction of biological targets for small molecule drugs. E3FP<sup>15</sup>, as the only one reported 3D molecular fingerprint, was inspired by ECFP and presents higher precision-recall performance than ECFP when integrated with SEA<sup>16</sup>. Besides fingerprints, Gaussian-based representation used by commercial software ROCS<sup>17</sup> is another vivid example that strengthen this argument. When it further comes to voxelized representation<sup>18, 19</sup>, it is a common practice to integrate this representation with supervised convolutional DNN and has demonstrated promising results on the prediction of the biological target or binding affinity for small molecule<sup>20-25</sup>. Despite this, there is no 3D fingerprint learned by DNN reported thus far.

Whereas 2D molecular fingerprints generated by DNN showed excellent ability in many predictive models, all such models reported up to now have two flaws: i) Training through supervised learning in specific tasks leads to inextensibility to newly emerging problems without sufficient labeled data; ii) Similarity calculation of such fingerprints is a complication to their compatibility with statistical models such as the similarity ensemble approach (SEA)<sup>16</sup>. Our research presented here is aimed to overcome these limitations and further push neural network to fingerprint 3D molecules.

3D molecule is a 3D object. Fingerprinting 3D molecule is encoding 3D object. We can learn a lot about the encoding method from computer graphics. Hinton et al. introduced CapsNet<sup>26, 27</sup> recently to learn to output the pose matrix of 3D objects, which can be intuitively interpreted as the orientation and position of objects in 3D space. Inspired by this, we construct a deep capsular neural network to fingerprint 3D small molecule, which can be trained without labeled data of specific predictive tasks. Given that one primary application of our fingerprint is ligand-based target prediction, molecular force fields grids, as a kind of voxelized representation, were adopted as the inputs of our neural network from 3D field-based QSAR<sup>28, 29</sup>, since the binding of small molecules to biological targets is dominated by physical forces. With a well-trained model, molecular force fields grids can be compressed into a pose matrix, termed as Three-dimensional Force Field Fingerprint (TF3P). TF3P demonstrates its stronger ability to capture 3D structural changes than other fingerprints and recognize similar targets that are inaccessible by other fingerprints based on only ligands similarity. Furthermore, TF3P is compatible with both statistical models and machine learning models. TF3P is anticipated to be a better choice of fingerprints for ligand-based drug discovery in the future. All codes for this model are written in Python and available at <https://github.com/canisw/tf3p>.

## Methods & Materials

### Model Architecture

Our model is a modified version of CapsNet, composed of 15 layers. The first 8 layers are encoder and the last 7 layers are decoder. The overall architecture is shown in **Figure 1**.

*Inputs.* Our model takes the force fields grids of a conformer of a molecule as inputs, which have two channels, namely van der Waals potential and electrostatic potential. The grids calculation is implemented using open source force field MMFF94<sup>30-34</sup> in Python with alkyl carbon and proton as probes for each channel, respectively. The box size is set to  $20 \times 20 \times 20$  Å, so that it can hold common lead-like small molecule drugs. The grids size is set to  $50 \times 50 \times 50$  points with a resolution of 0.4 Å. In summary, the input tensor for each conformer has the shape of  $2 \times 50 \times 50 \times 50$ .

*Encoder.* This part of the network takes the input force fields grids and learns to encode them into a  $166 \times 8$  matrix as the fingerprint. The encoder consists of six 3D convolutional layers and two capsular layers. The convolutional layers serve as feature extractor to reduce the sparse inputs’ dimension into a smaller size suitable for the subsequent capsular layers, since capsular layer has hundreds times of trainable parameters than convolutional layer under the same scale. Every convolutional layer has kernels with size of  $3 \times 3 \times 3$  and stride 1, followed by batch normalization and LeakyReLU activation. Besides, in every two convolutional layers is inserted a max pooling layer. After convolution, the inputs’ shape is transformed into  $128 \times 5 \times 5 \times 5$ . PrimaryCaps layer is in nature a convolutional layer with its scalar outputs chunked into vectors and then squashed. The squashing function is the novel non-linear activation function designed for capsules. DigitCaps layer receives input from all the capsules in PrimaryCaps layer with routing by agreement and produces a matrix with size of  $166 \times 8$ .

*Decoder.* The decoder part takes the outputs of DigitCaps, the fingerprint, to reconstruct the input force fields grids. This part is used as a regularizer, whose job is to encourage the digit capsules to encode the pose information into each digit. Therefore, we simply use a nearly symmetric architecture consisting of a linear layer, transposed 3D convolutional layers with upsampling to decode the outputs of DigitCaps.

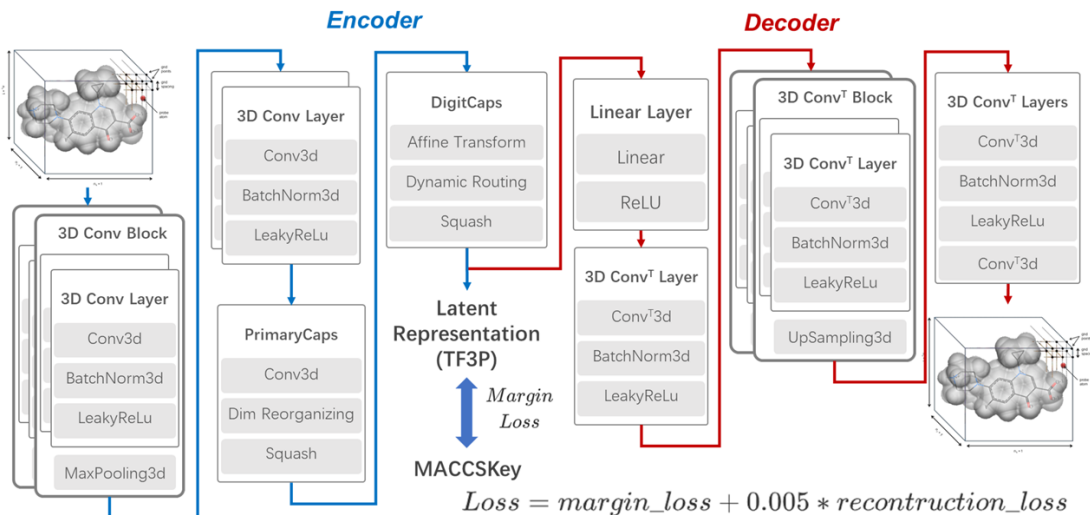


**Figure 1.** The architecture of our model.

## Model Training

Our model was implemented with Pytorch 1.3<sup>35</sup> and trained with Adam<sup>36</sup> optimizer. The learning rate was set to 0.001, and all other parameters was default. The loss function we used was same to that of CapsNet, which has two parts: Margin loss and reconstruction loss.

$$Loss = margin\_loss + 0.005 * reconstruction\_loss$$

Where the margin loss used 2D molecular fingerprints as labeled digit class, and the reconstruction loss used MSE loss. To make the training feasible in a relative short period of time and the results

comparable, MACCSKey and ECFP4 used here for training were both 166-bits binary fingerprints. The final model for evaluation was trained on 1% random samples of the full prepared training set. The training process took up to about one week on three NVIDIA TITAN RTX GPUs.

## Data set

*ZINC15*<sup>37</sup> 3D lead-like ( $\log P \leq 3.5$ ,  $250 < MW < 500$ ) subset was retrieved to train our model. A total number of ~286 million molecules with pre-generated conformer was downloaded from ZINC database. Approximately 25 thousand molecules (less than 0.01%) that cannot be parameterized by MMFF94 force field and cannot be sanitized by RDKit (v2019.09.2)<sup>38, 39</sup> were filtered out and excluded from the subsequent training process. However, given the huge calculation cost of force fields grids and the large size of the data set, not all of these data were actually used in the study. We randomly sampled various proportion of the full data set and split it randomly into training set and test set by 9:1 for model training.

*ChEMBL25*<sup>40, 41</sup> were retrieved for the evaluation. The distribution of the number of rotatable bonds of all molecules in ChEMBL25 were analyzed. For the assessment of fingerprints’ sensitivity to 3D structural changes, 1000 molecules were randomly sampled for each number of rotatable bonds ranging from 0 to 15. One reference conformer and 10 more conformers for each molecule were generated and each of the ten conformers was aligned to the reference to calculate RMSD and similarities. All of this implemented with RDKit.

*PDBBind v2018 General Set*<sup>42</sup> were retrieved for the evaluation. All the complexes with pActivity ( $pK_d$ ,  $pIC_{50}$ , etc.) greater than 6 were kept as “active” samples and only this subset was used. The conformers of ligands from the crystal structures were prepared and used for fingerprints calculation.

*The dataset for solubility and malaria bioactivity prediction* was benchmarked by Duvenaud et al.<sup>13</sup> and Kearnes et al.<sup>43</sup>

## Fingerprints calculation

Except that 166-bits ECFP4 was used in the model training, 1024-bits one was utilized for all the evaluation. Both ECFP4 and MACCSKey were computed using RDKit. 1024-bits E3FP was computed using the default parameters and the codes were provided by the author in his Github repo ([https://github.com/keiserlab/e3fp-paper/tree/1.1/e3fp\\_paper](https://github.com/keiserlab/e3fp-paper/tree/1.1/e3fp_paper)).

## Results & Discussion

### A novel 3D fingerprint and its similarity calculation

During the training process, 2D fingerprints were used as digit class label, as each digit represents a certain 2D structural feature. Under this circumstance, each digit capsule had to learn to output an eight-dimensional vector containing the 3D force fields information in regard to each 2D structural feature. We assessed the training performance with two commonly applied 2D fingerprints, namely MACCSKey and ECFP4.

As shown in **Figure 2**, more data was fed into the model, lower did the loss value achieve. An interesting point is that the loss value decreases to almost the same after the same amount of the total fed data, no matter what proportion of the full dataset sampled. This indicates a great structural redundancy of the ZINC database. Compared with MACCSKey, the loss value convergent pretty slowly when training with 166-bits ECFP4. In summary, 1% of the full dataset is sufficient for the convergence of the loss function after 10 epochs of training with MACCSKey. This model was used to generate TF3P of molecules in the following evaluation.

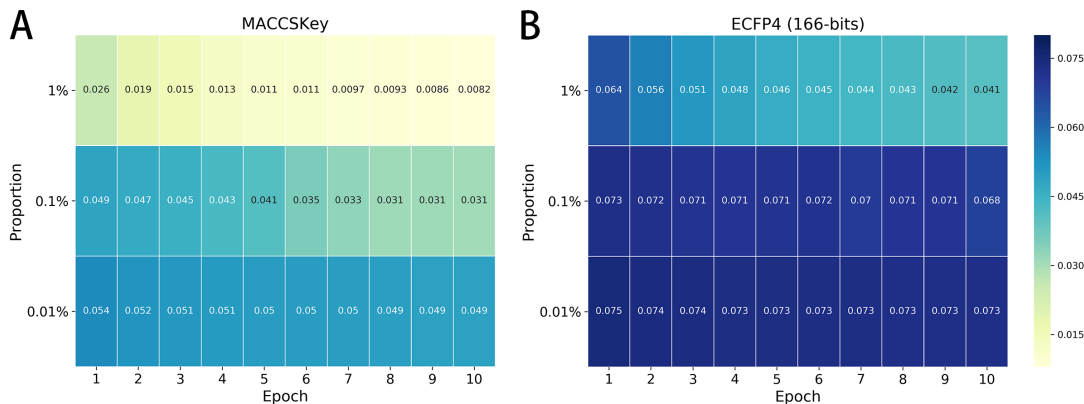


**Figure 2.** Training performance with different fingerprints and various proportions of the full dataset retrieved from ZINC15 3D lead-like subset. A) The loss value of test set when training with MACCSKey. B) The loss value of test set when training with 166-bits ECFP4.

Similarity calculation of classical binary fingerprints commonly executed with Tanimoto coefficient, which does not work for real-valued fingerprints, i.e. TF3P. Since TF3P is a matrix of which each row vector has its independent structural meaning, it is intuitive to calculate the similarity row-wisely. We designed a weighted mean of the cosine similarity of each row vector to calculate the similarity between two TF3Ps,  $\mathbf{M}$ ,  $\mathbf{N} \in \mathbb{R}^{K \times L}$ , as the following form:

$$Sim = \left( \frac{1}{2k} \sum_k ((1 - |m_k - n_k|) \frac{p_k}{m_k n_k} + 1) \right)^3$$

where  $\mathbf{p}$ ,  $\mathbf{m}$ ,  $\mathbf{n} \in \mathbb{R}^K$ ,  $p_k = \sum_l M_{kl} N_{kl}$ ,  $m_k = \sqrt{\sum_l M_{kl}^2}$ ,  $n_k = \sqrt{\sum_l N_{kl}^2}$ .

### Capturing 3D structural changes of molecules

The basic virtue of 3D fingerprint is the capability to discriminate different conformers of a molecule. To assess fingerprints’ ability to capture conformational changes, we sampled thousands of molecules with the number of rotatable bonds ranging from 0 to 15 (This range was determined by the distribution of the number of rotatable bonds in ChEMBL25, **Figure S1**). The RMSD values and similarity by fingerprints between different conformers of each molecule were calculated. As the number of rotatable bonds increases, the mean RMSD rises, denoting growing conformational space of molecule (**Figure 3 A and B, Table S1**). 2D fingerprints unable to encode 3D conformational information produce similarity values of one for all entries (**Table S1**). The sole existing 3D fingerprint, E3FP, do have the ability to apprehend 3D conformational changes, yielding decreasing similarities with the increasing mean RMSD (**Figure 3 B**). Nevertheless, TF3P is more sensitive to the 3D conformational changes, demonstrated by a stronger correlation of similarity vs. RMSD than E3FP, measured by Pearson’s r coefficient (**Figure 3 A**). In addition, it is strange that some pairs of conformers with very low RMSD yield low similarities by E3FP (Down left in **Figure 3 B**).

Two examples illustrated what discussed above. **CHEMBL4116653** can undergoes conformational isomerization because of its freely rotatable single bonds (**Figure 3 C**). Among three conformers of **CHEMBL4116653**, conf\_1 are very similar to conf\_2 but far dissimilar to conf\_3, indicated by the divergence in RMSD values. The similarities by TF3P are consistent with this divergence, but not by E3FP. Another case is a series of natural products with four chiral carbons<sup>44</sup>, a pair of enantiomers plus a structural isomer (**Figure 3 D**). 2D fingerprints encounter bafflement when distinguishing between a pair of enantiomers, **Anti-hh** and **Anti-hh’**. Since they are isomers, the RMSD values among them can be calculated to indicate the 3D conformational deviation. Similar situations occur for TF3P and E3FP, respectively: The similarity by E3FP hardly changes, whereas

the similarity by TF3P shifts accordingly with the RMSD. Taken together, TF3P is more sensitive to the 3D structural differences of molecules, regardless of the 2D topology or configuration.

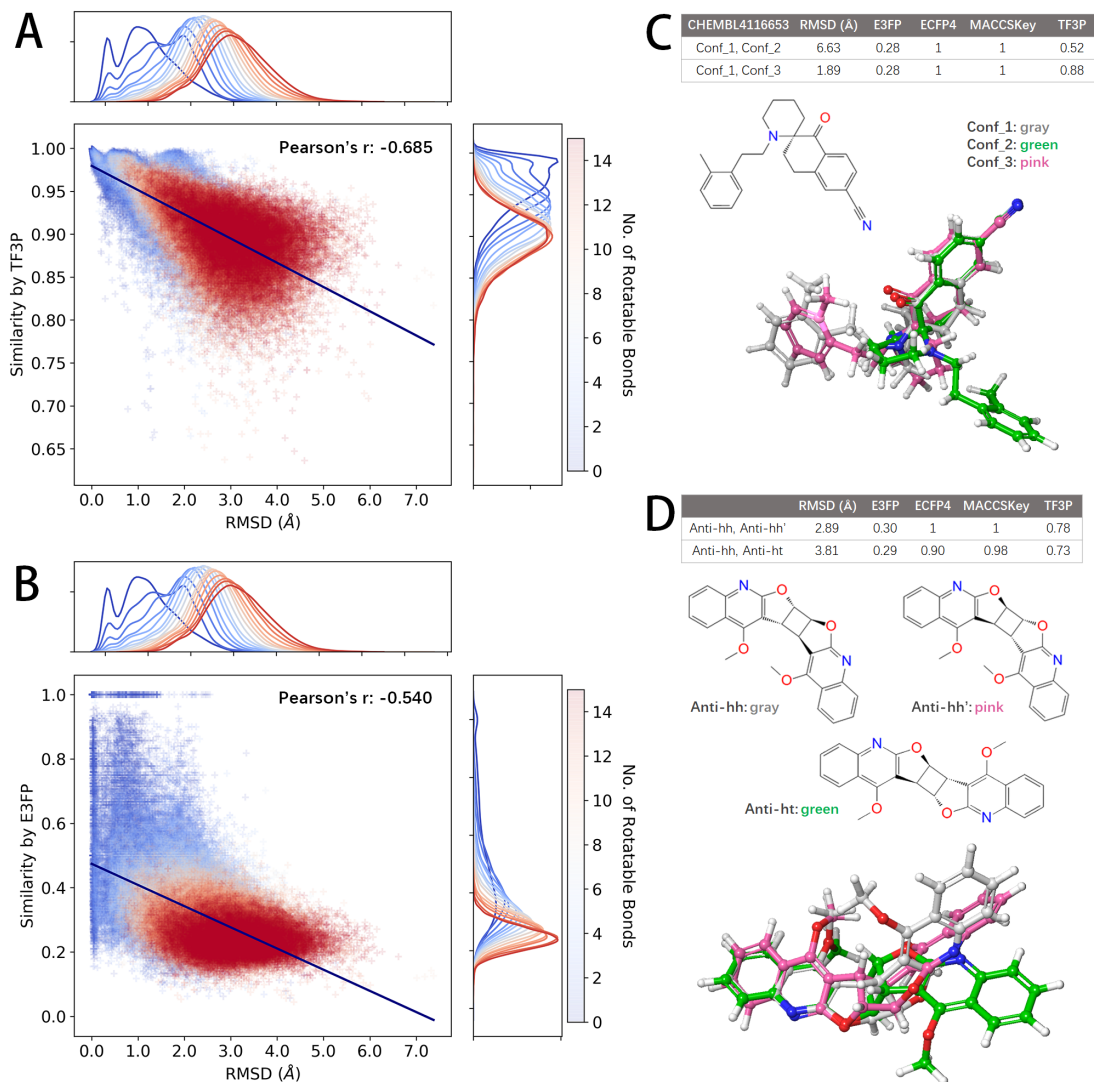


**Figure 3.** Capturing 3D structural changes of molecules. A, B) The correlation between similarity and RMSD for TF3P and E3FP. Each point represents a pair of conformers belonging to a molecule, colored by the number of rotatable bonds of that molecule. C, D) Two examples with RMSD, similarities, 2D structures and 3D aligned conformers.

### Finding similar pockets by similar ligands

The primary intuition of using molecular 3D force fields grids has two aspects. On the one hand, force fields contain the raw information dominating the interaction between drugs and targets; on the other hand, force fields are degenerate of atom types and bonds of molecular graph representation. TF3P, as a fingerprint derived from force fields, therefore, was expected to be capable to recognize molecule pairs that is dissimilar in 2D topology but resemble each other in 3D shape and electrostatics. Given the 3D complementation between the ligands and the pockets they bind to, this is deemed to improve the precision of the targets similarity inference based on ligands similarity, which is the essence of similarity-based target prediction. In this study, targets similarity was represented by FuzCav pockets similarity<sup>45</sup>, with particular emphasis on the binding. PDBBind v2018 General Set was selected to

study the inference further, in consideration of ruling out bad effects resulting from conformation sampling strategy.

As shown in **Table 1**, the overall (Top 100%) Pearson’s r coefficients of FuzCav similarity vs. the similarity by all fingerprints are extremely low, suggesting the toughness to perfectly infer target similarity from only ligands information. Nevertheless, it is noteworthy that the correlations are generally higher in top ranked samples by similarity than bottom ranked ones with no exception. The same situation occurs in Spearman’s r (**Table 2**) and Kendall’s tau (**Table S2**) coefficients. This is probably resulted from that subtle differences between similar ligands correspond to a similar degree of conformational changes between pockets and thus presenting correlations easy to fit for top ranked pairs by fingerprints similarity. However, in contrast to similar ligands binding to pockets alike, every ligand dissimilar to others binds to its target in its own way, causing complications to the regression for dissimilar pairs. As for top ranked pairs, good correlations only mean similar orders in two arrays of samples, not the exact values. We further analyzed the average values of FuzCav similarities of samples with incrementing ranking thresholds. As shown in **Figure 4 A**, top ranked pairs by TF3P similarity present significant higher average FuzCav pocket similarities than those by E3FP and 2D fingerprints. Taken together, compared to other fingerprints, similar ligands found by TF3P do bind to similar targets and their ligand similarity is a better indicator of the pocket similarity.

**Table 1.** Pearson’s r of FuzCav similarity vs. different fingerprints similarity for all active pairs from PDDBind v2018 General Set.

Top % <sup>a</sup>	TF3P	E3FP	MACCSKey	ECFP4
0.5	<b>0.52*</b>	0.29	0.34	0.31
1	<b>0.47*</b>	0.30	0.32	0.29
5	0.24	<b>0.25*</b>	0.20	0.24
10	0.17	<b>0.22*</b>	0.14	0.21
20	0.12	<b>0.19*</b>	0.10	0.18
50	0.07	<b>0.15*</b>	0.08	0.14
100	0.08	<b>0.13*</b>	0.10	0.11

<sup>a</sup>: Sorted by the indicated fingerprint similarity.

**Table 2.** Spearman’s r of FuzCav similarity vs. different fingerprints similarity for all active pairs from PDDBind v2018 General Set.

Top % <sup>a</sup>	TF3P	E3FP	MACCSKey	ECFP4
0.5	<b>0.33*</b>	0.16	0.18	0.19
1	<b>0.20*</b>	0.12	0.12	0.11
5	-0.01	<b>0.08*</b>	0.01	0.03
10	-0.03	<b>0.07*</b>	0.00	0.02
20	-0.03	<b>0.07*</b>	0.01	0.01
50	-0.00	<b>0.07*</b>	0.03	0.02
100	0.04	<b>0.08*</b>	<b>0.08*</b>	0.04

<sup>a</sup>: Sorted by the indicated fingerprint similarity.

In fact, we only pay attention to top ranked outputs in real scenario of ligand-based drug discovery. Like the early stage enrichment is of more importance for virtual screening, we also need a stronger “early stage enrichment” for target prediction based on only ligands similarity. This is to say, a good fingerprint for ligand-based target prediction need have the ability to rank the targets whose pockets are similar to the true target at the top of the targets pool and with an order that is well correlated



to their pockets similarity. To this end, TF3P outperforms the solely existing 3D fingerprint E3FP and 2D fingerprints, ECFP4 and MACCSKey.

Here, we also show three examples among the most similar pairs by TF3P that do not resemble by other fingerprints (**Figure 4 B, C and D**). Each pair binds to the same target. As the similarity values calculated by different fingerprints over the same dataset show divergent distributions (**Figure S2**), the percentile ranks were computed and attached below the exact values of similarity to demonstrate how similar different fingerprints regard them. As shown in the aligned crystal structures (**Figure 4 B, C and D**), all three pairs have obviously similar 3D force fields but dissimilar in 2D topology. This leads to difficulty to recognize their resemblance for the existing fingerprints based on topological structure but not for TF3P that is derived from 3D force fields. Therefore, TF3P can rank these pairs at the top places (Top 1%) based on ligands similarity but others cannot.

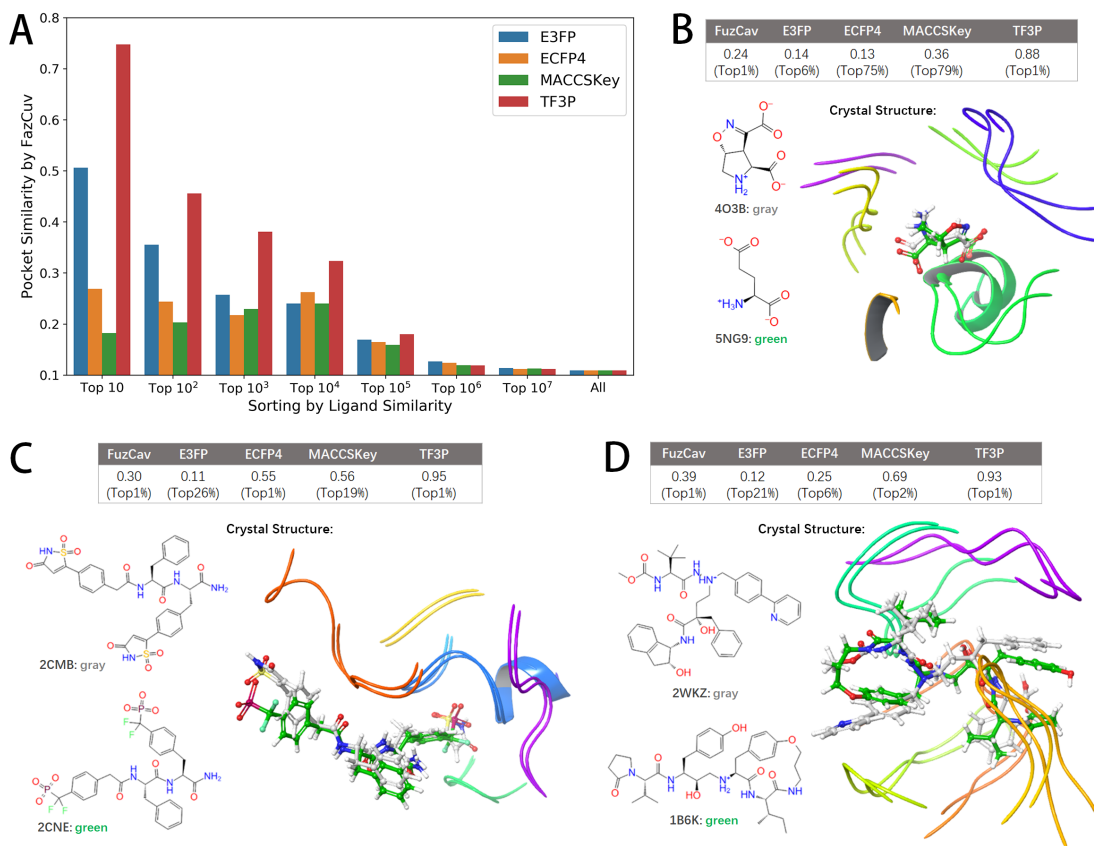


**Figure 4.** Finding similar pockets by similar ligands. A) Average pocket similarity for samples with incrementing cutoffs in ranking (Top 1% is equivalent to top 10<sup>5</sup>). B, C, D) Three top ranked similar pairs by TF3P but are inaccessible by other fingerprints.

### SEA analysis of PDDBind database

SEA is a widely used statistical model that quantitatively groups and relates proteins based on the chemical similarity of their ligands. We utilized SEA to analyze all targets that annotated no less than 10 active complexes within PDDBind v2018 General Set with four fingerprints, namely TF3P, E3FP, MACCSKey and ECFP4. The results demonstrate a similar trend to the above study: TF3P can enrich more pairs of the targets that resemble each other by pocket similarity in the targets pool (**Figure 5 A**), indicating TF3P as a better choice for SEA-based target prediction, compared to other fingerprints.

One primary application of SEA is to cluster proteins using only ligands similarity to find some links unexpected. First, it is not beyond anticipation that TF3P outputs a clustering of targets closer to FuzCav similarity, measured by adjusted Rand score (**Figure 5 B**). Moreover, some interesting links indeed emerged when we conducted SEA analysis with TF3P (**Figure 5 C**). The first one is a cluster of HIV relevant proteins, including HIV protease, HIV integrase, and HIV reverse transcriptase, which are highly pharmacologically related. The second one is endothiapsin (Uniprot ID: P11838) from *Cryptosporidium parvum* and plasmepsin-2 (Uniprot ID: P46925) from *Plasmodium falciparum*, which function similarly as aspartic-type endopeptidase although they are from different organisms. The third one is retinoic acid receptor RXR-alpha (Uniprot ID: P19793) and peroxisome proliferator-activated receptor gamma (Uniprot ID: P37231), which are not only biologically related but also have very similar 3D structure of the ligand binding domain (**Figure 5 D**). Notably, the latter two did not emerge when using E3FP and 2D fingerprints (**Figure S3**).

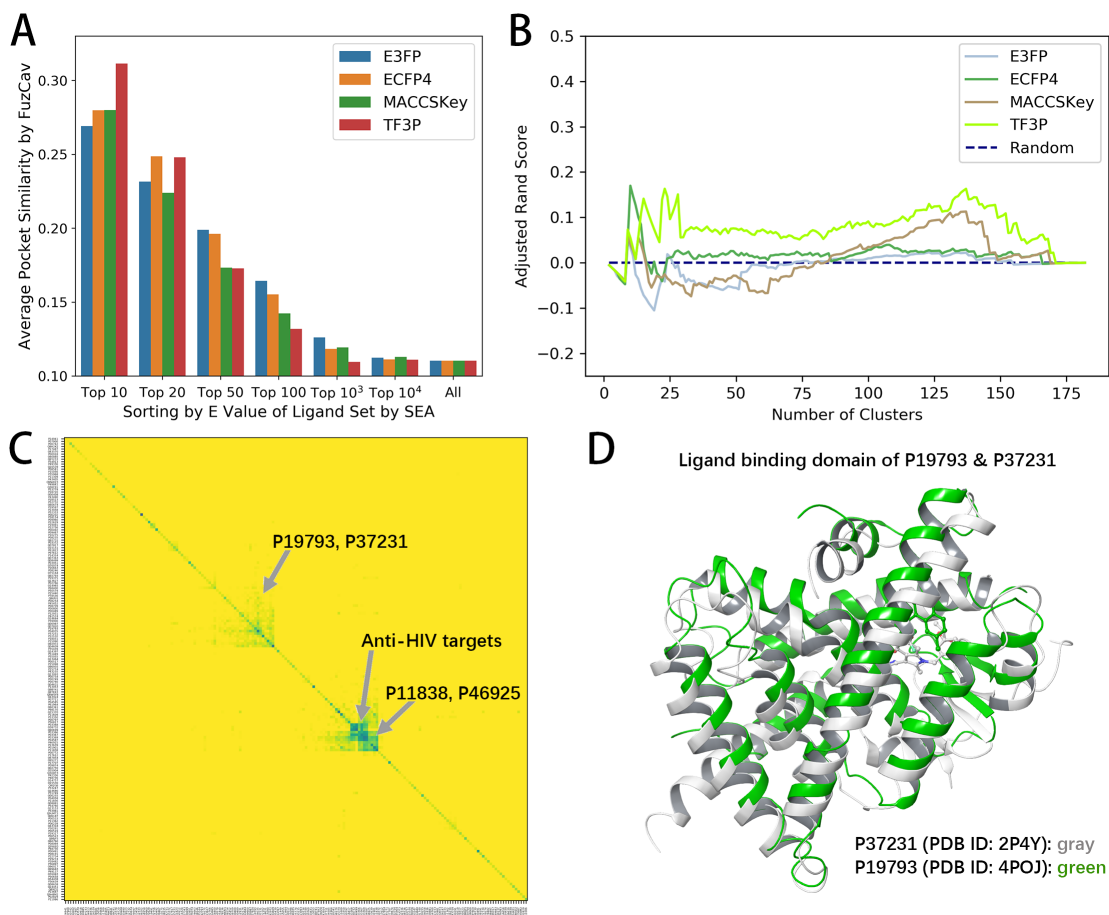


**Figure 5.** SEA analysis of PDBBind database. A) Average pocket similarity for targets pairs with incrementing cutoffs in ranking. B) The distance of FuzCav clustering of targets to clustering by four fingerprints, measured by adjusted Rand score. C) Heatmap of E-value of indicated targets calculated by SEA. For high-resolution images, see <https://github.com/canisw/tf3p/tree/master/images>. D) Aligned crystal structures of ligand binding domains of two indicated targets.

### Application with machine learning models

Aside from calculate similarity between two molecules, another important application of fingerprints is to be used as the inputs for machine learning models. To this end, we used a very simple model, single linear layer neural network to assess the performance of different fingerprints on several tasks.

TF3P achieves the lowest MSE value in 5-fold cross validation among all of the four fingerprints on solubility prediction and outperforms E3FP on malaria bioactivity prediction, demonstrating its promising capability when integrated with machine learning models.

**Table 3.** Prediction of solubility and malaria bioactivity with different fingerprints.

Fingerprint	Solubility <sup>a</sup> log10 (mol/L)	Malaria bioactivity <sup>a</sup> ln ( $\mu$ mol/L)
MACCSKey + Linear layer	1.33 $\pm$ 0.20	1.22 $\pm$ 0.03
ECFP4 + Linear layer	1.71 $\pm$ 0.27	<b>1.14 <math>\pm</math> 0.03*</b>
E3FP + Linear layer	1.71 $\pm$ 0.27	1.34 $\pm$ 0.06
TF3P + Linear layer	<b>0.66 <math>\pm</math> 0.09*</b>	1.27 $\pm$ 0.08

<sup>a</sup>: Evaluation matrix: mean  $\pm$  std. of MSE

## Conclusion

In summary, we developed a new fingerprint of 3D molecule with deep capsular network, which learned to encode the 3D force fields information into each digit of 2D fingerprint without labeled data for specific predictive tasks. The fingerprint produced by our model, TF3P, is easy to calculate similarity and thus compatible with statistical models. Also, TF3P could be applied with machine learning models as the inputs and present promising results. Since TF3P is derived from molecular 3D force fields, it demonstrated its ability to recognize molecule pairs that is dissimilar in 2D topology but resemble each other in 3D shape and electrostatics, which improves its ability to infer pockets similarity based on only ligands similarity, yielding pairs of ligands with similar targets inaccessible by other fingerprints. Further development and benchmarking studies of TF3P-based target prediction software is still going on.

## Supplementary Information

Supplementary Information: Supplementary figures and tables.

## Acknowledgments

This research was supported by the National Natural Science Foundation of China (Grant numbers 21572010, 21772005), National Major Scientific and Technological Special Project for Significant New Drugs Development 843 (2019ZX09204-001) and Beijing Natural Science Foundation (7172118).

## Abbreviations used

placeholder

## Declaration of interest

The authors report no conflicts of interest. The authors alone are responsible for the content and writing of this article.

## References

1. Boström, J.; Hogner, A.; Schmitt, S., Do Structurally Similar Ligands Bind in a Similar Fashion? *Journal of Medicinal Chemistry* **2006**, 49, 6716-6725.
2. Karelson, M.; Lobanov, V. S.; Katritzky, A. R., Quantum-Chemical Descriptors in QSAR/QSPR Studies. *Chemical Reviews* **1996**, 96, 1027-1044.
3. Todeschini, R.; Consonni, V., *Handbook of molecular descriptors*. WileyVCH, Weinheim. 2000; Vol. 11.
4. Jiang, P.; Saydam, S.; Ramandi, H. L.; Crosky, A.; Maghrebi, M. Deep Molecular Representation in Cheminformatics. In *Handbook of Deep Learning Applications*, Balas, V. E.; Roy, S. S.; Sharma, D.; Samui, P., Eds.; Springer International Publishing: Cham, 2019, pp 147-159.
5. Li, X.; Li, Z.; Wu, X.; Xiong, Z.; Yang, T.; Fu, Z.; Liu, X.; Tan, X.; Zhong, F.; Wan, X.; Wang, D.; Ding, X.; Yang, R.; Hou, H.; Li, C.; Liu, H.; Chen, K.; Jiang, H.; Zheng, M., Deep Learning Enhancing Kinome-Wide Polypharmacology Profiling: Model Construction and Experiment Validation. *Journal of Medicinal Chemistry* **2019**.
6. Durant, J. L.; Leland, B. A.; Henry, D. R.; Nourse, J. G., Reoptimization of MDL Keys for Use in Drug Discovery. *Journal of Chemical Information and Computer Sciences* **2002**, 42, 1273-1280.
7. Rogers, D.; Hahn, M., Extended-Connectivity Fingerprints. *Journal of Chemical Information and Modeling* **2010**, 50, 742-754.
8. Huo, H.; Rupp, M., Unified representation of molecules and crystals for machine learning. *arXiv preprint arXiv:1704.06439* **2017**.
9. Schütt, K. T.; Arbabzadah, F.; Chmiela, S.; Müller, K. R.; Tkatchenko, A., Quantum-chemical insights from deep tensor neural networks. *Nature Communications* **2017**, 8, 13890.
10. Lubbers, N.; Smith, J. S.; Barros, K., Hierarchical modeling of molecular energies using a deep neural network. *The Journal of Chemical Physics* **2018**, 148, 241715.
11. Schütt, K. T.; Sauceda, H. E.; Kindermans, P. J.; Tkatchenko, A.; Müller, K. R., SchNet - A deep learning architecture for molecules and materials. *The Journal of Chemical Physics* **2018**, 148, 241722.
12. Xiong, Z.; Wang, D.; Liu, X.; Zhong, F.; Wan, X.; Li, X.; Li, Z.; Luo, X.; Chen, K.; Jiang, H.; Zheng, M., Pushing the Boundaries of Molecular Representation for Drug Discovery with the Graph Attention Mechanism. *Journal of Medicinal Chemistry* **2019**.
13. Duvenaud, D. K.; Maclaurin, D.; Iparraguirre, J.; Bombarell, R.; Hirzel, T.; Aspuru-Guzik, A.; Adams, R. P. Convolutional networks on graphs for learning molecular fingerprints. In *Advances in neural information processing systems*, 2015; 2015; pp 2224-2232.
14. Shin, W.-H.; Zhu, X.; Bures, G. M.; Kihara, D., Three-Dimensional Compound Comparison Methods and Their Application in Drug Discovery. *Molecules* **2015**, 20.
15. Axen, S. D.; Huang, X.-P.; Cáceres, E. L.; Gendele, L.; Roth, B. L.; Keiser, M. J., A Simple Representation of Three-Dimensional Molecular Structure. *Journal of Medicinal Chemistry* **2017**, 60, 7393-7409.
16. Keiser, M. J.; Roth, B. L.; Armbruster, B. N.; Ernsberger, P.; Irwin, J. J.; Shoichet, B. K., Relating protein pharmacology by ligand chemistry. *Nature Biotechnology* **2007**, 25, 197-206.
17. Hawkins, P. C. D.; Skillman, A. G.; Nicholls, A., Comparison of Shape-Matching and Docking as Virtual Screening Tools. *Journal of Medicinal Chemistry* **2007**, 50, 74-82.
18. Fontaine, F.; Bolton, E.; Borodina, Y.; Bryant, S. H., Fast 3D shape screening of large chemical databases through alignment-recycling. *Chemistry Central Journal* **2007**, 1, 12.

19. Koes, D. R.; Camacho, C. J., Shape-based virtual screening with volumetric aligned molecular shapes. *Journal of Computational Chemistry* **2014**, *35*, 1824-1834.
20. Wallach, I.; Dzamba, M.; Heifets, A., AtomNet: A Deep Convolutional Neural Network for Bioactivity Prediction in Structure-based Drug Discovery. *arXiv.org* **2015**, 1510.02855.
21. Gomes, J.; Ramsundar, B.; Feinberg, E. N.; Pande, V. S. Atomic Convolutional Networks for Predicting Protein-Ligand Binding Affinity. *arXiv e-prints*2017; <https://ui.adsabs.harvard.edu/> (accessed March 01, 2017).
22. Jiménez, J.; Škalič, M.; Martínez-Rosell, G.; De Fabritiis, G., KDEEP: Protein-Ligand Absolute Binding Affinity Prediction via 3D-Convolutional Neural Networks. *Journal of Chemical Information and Modeling* **2018**, *58*, 287-296.
23. Ragoza, M.; Hochuli, J.; Idrobo, E.; Sunseri, J.; Koes, D. R., Protein-Ligand Scoring with Convolutional Neural Networks. *Journal of Chemical Information and Modeling* **2017**, *57*, 942-957.
24. Skalic, M.; Jiménez, J.; Sabbadin, D.; De Fabritiis, G., Shape-Based Generative Modeling for de Novo Drug Design. *Journal of Chemical Information and Modeling* **2019**, *59*, 1205-1214.
25. Golkov, V.; Skwark, M. J.; Mirchev, A.; Dikov, G.; Geanes, A. R.; Mendenhall, J.; Meiler, J.; Cremers, D., 3D deep learning for biological function prediction from physical fields. *arXiv preprint arXiv:1704.04039* **2017**.
26. Hinton, G. E.; Krizhevsky, A.; Wang, S. D. Transforming Auto-Encoders. In *Artificial Neural Networks and Machine Learning - ICANN 2011, Berlin, Heidelberg, 2011//*, 2011; Honkela, T.; Duch, W.; Girolami, M.; Kaski, S., Eds. Springer Berlin Heidelberg: Berlin, Heidelberg, 2011; pp 44-51.
27. Sabour, S.; Frosst, N.; Hinton, G. E. Dynamic routing between capsules. In *Advances in neural information processing systems*, 2017; 2017; pp 3856-3866.
28. Cramer, R. D.; Patterson, D. E.; Bunce, J. D., Comparative molecular field analysis (CoMFA). 1. Effect of shape on binding of steroids to carrier proteins. *Journal of the American Chemical Society* **1988**, *110*, 5959-5967.
29. Klebe, G.; Abraham, U.; Mietzner, T., Molecular similarity indices in a comparative analysis (CoMSIA) of drug molecules to correlate and predict their biological activity. *Journal of medicinal chemistry* **1994**, *37*, 4130-4146.
30. Halgren, T., Merck Molecular Force Field. III. Molecular geometries and vibrational frequencies for MMFF94. *Journal of Computational Chemistry* **1996**, *17*, 553-586.
31. Halgren, T., Merck Molecular Force Field. V. Extension of MMFF94 using experimental data, additional computational data, and empirical rules. *Journal of Computational Chemistry* **1996**, *17*, 616-641.
32. Halgren, T. A., Merck molecular force field. I. Basis, form, scope, parameterization, and performance of MMFF94. *Journal of Computational Chemistry* **1996**, *17*, 490-519.
33. Halgren, T. A., Merck molecular force field. II. MMFF94 van der Waals and electrostatic parameters for intermolecular interactions. *Journal of Computational Chemistry* **1996**, *17*, 520-552.
34. Tosco, P.; Stiefl, N.; Landrum, G., Bringing the MMFF force field to the RDKit: implementation and validation. *Journal of Cheminformatics* **2014**, *6*, 37.
35. Paszke, A.; Gross, S.; Massa, F.; Lerer, A.; Bradbury, J.; Chanan, G.; Killeen, T.; Lin, Z.; Gimelshein, N.; Antiga, L.; Desmaison, A.; Köpf, A.; Yang, E.; DeVito, Z.; Raison, M.; Tejani, A.; Chilamkurthy, S.; Steiner, B.; Fang, L.; Chintala, S., *PyTorch: An Imperative Style, High-Performance Deep Learning Library*. 2019.
36. Kingma, D.; Ba, J., Adam: A Method for Stochastic Optimization. *International Conference on Learning Representations* **2014**.

37. Sterling, T.; Irwin, J. J., ZINC 15 - Ligand Discovery for Everyone. *Journal of Chemical Information and Modeling* **2015**, 55, 2324-2337.
38. Landrum, G. *RDKit: Open-source cheminformatics*.
39. Lovrić, M.; Molero, J. M.; Kern, R., PySpark and RDKit: Moving towards Big Data in Cheminformatics. *Molecular Informatics* **2019**, 38, 1800082.
40. Davies, M.; Nowotka, M.; Papadatos, G.; Dedman, N.; Gaulton, A.; Atkinson, F.; Bellis, L.; Overington, J. P., ChEMBL web services: streamlining access to drug discovery data and utilities. *Nucleic Acids Research* **2015**, 43, W612-W620.
41. Gaulton, A.; Hersey, A.; Nowotka, M.; Bento, A. P.; Chambers, J.; Mendez, D.; Mutowo, P.; Atkinson, F.; Bellis, L. J.; Cibrián-Uhalte, E.; Davies, M.; Dedman, N.; Karlsson, A.; Magariños, M. P.; Overington, J. P.; Papadatos, G.; Smit, I.; Leach, A. R., The ChEMBL database in 2017. *Nucleic Acids Research* **2016**, 45, D945-D954.
42. Liu, Z.; Su, M.; Han, L.; Liu, J.; Yang, Q.; Li, Y.; Wang, R., Forging the Basis for Developing Protein-Ligand Interaction Scoring Functions. *Accounts of Chemical Research* **2017**, 50, 302-309.
43. Kearnes, S.; McCloskey, K.; Berndl, M.; Pande, V.; Riley, P., Molecular graph convolutions: moving beyond fingerprints. *Journal of Computer-Aided Molecular Design* **2016**, 30, 595-608.
44. Gao, P.; Wang, L.; Zhao, L.; Zhang, Q.-y.; Zeng, K.-w.; Zhao, M.-b.; Jiang, Y.; Tu, P.-f.; Guo, X.-y., Anti-inflammatory quinoline alkaloids from the root bark of *Dictamnus dasycarpus*. *Phytochemistry* **2019**, In press.
45. Weill, N.; Rognan, D., Alignment-Free Ultra-High-Throughput Comparison of Druggable Protein-Ligand Binding Sites. *Journal of Chemical Information and Modeling* **2010**, 50, 123-135.

## Supporting Information

### TF3P: Three-dimensional Force Fields Fingerprint Learned by Deep Capsular Network

Yanxing Wang<sup>†</sup>, Jianxing Hu<sup>†</sup>, Junyong Lai, Yibo Li, Hongwei Jin, Lihe Zhang, Liangren Zhang<sup>\*</sup>, Zhenming Liu<sup>\*</sup>

State Key Laboratory of Natural and Biomimetic Drugs, School of Pharmaceutical Sciences, Peking University, Beijing, 100191, P. R. China

<sup>†</sup>: These authors contribute equally.

<sup>\*</sup>: To whom correspondence should be addressed.

#### Contents:

**Figure S1.** The distribution of the number of rotatable bonds in ChEMBL. 2

**Figure S2.** The distributions of similarity by different fingerprints of over the active pairs sampled from PDDBind v2018 General Set. 3

**Figure S3.** Heatmap of E-value of indicated targets calculated by SEA with four fingerprints. 4

**Table S1.** RMSD vs. similarity by TF3P, E3FP and 2D FPs. 5

**Table S2.** Kendall's tau of FuzCav similarity vs. different fingerprints similarity for all active pairs from PDDBind v2018 General Set. 6

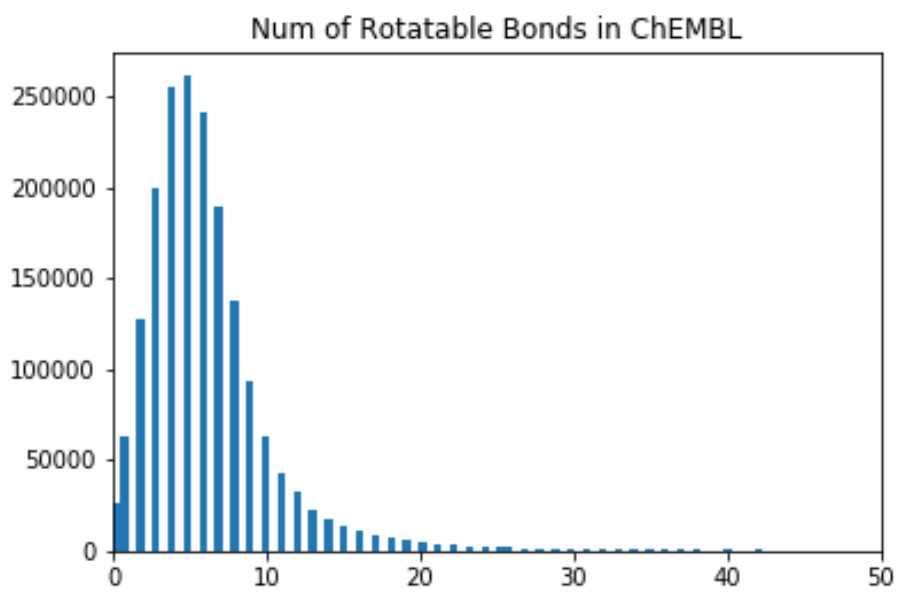


**Figure S1.** The distribution of the number of rotatable bonds of molecules in ChEMBL.



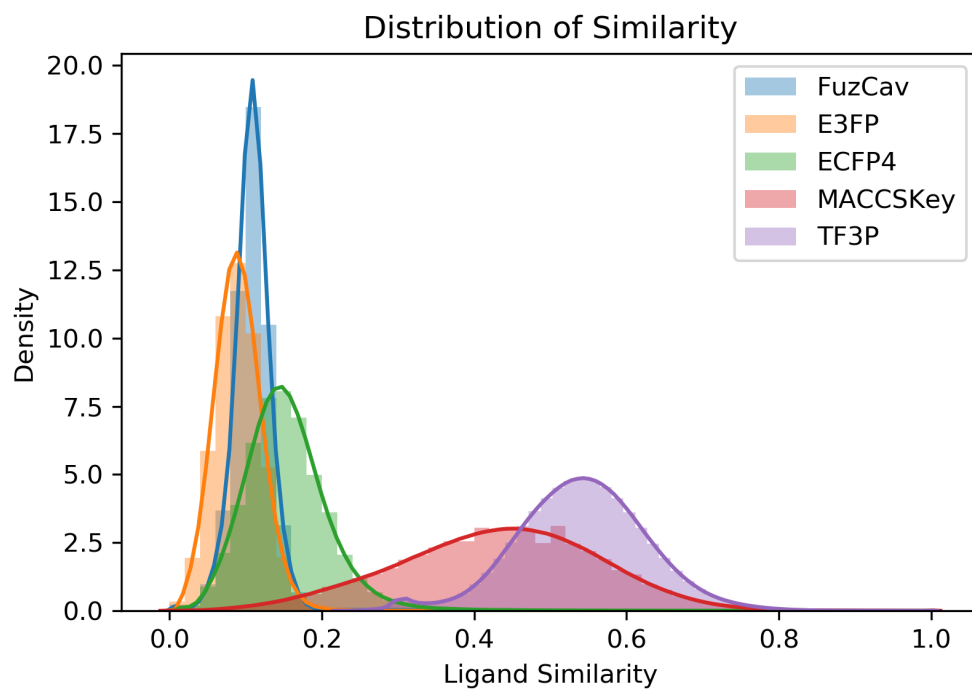


**Figure S2.** The distributions of similarity by different fingerprints of over the active pairs sampled from PDBBind v2018 General Set.

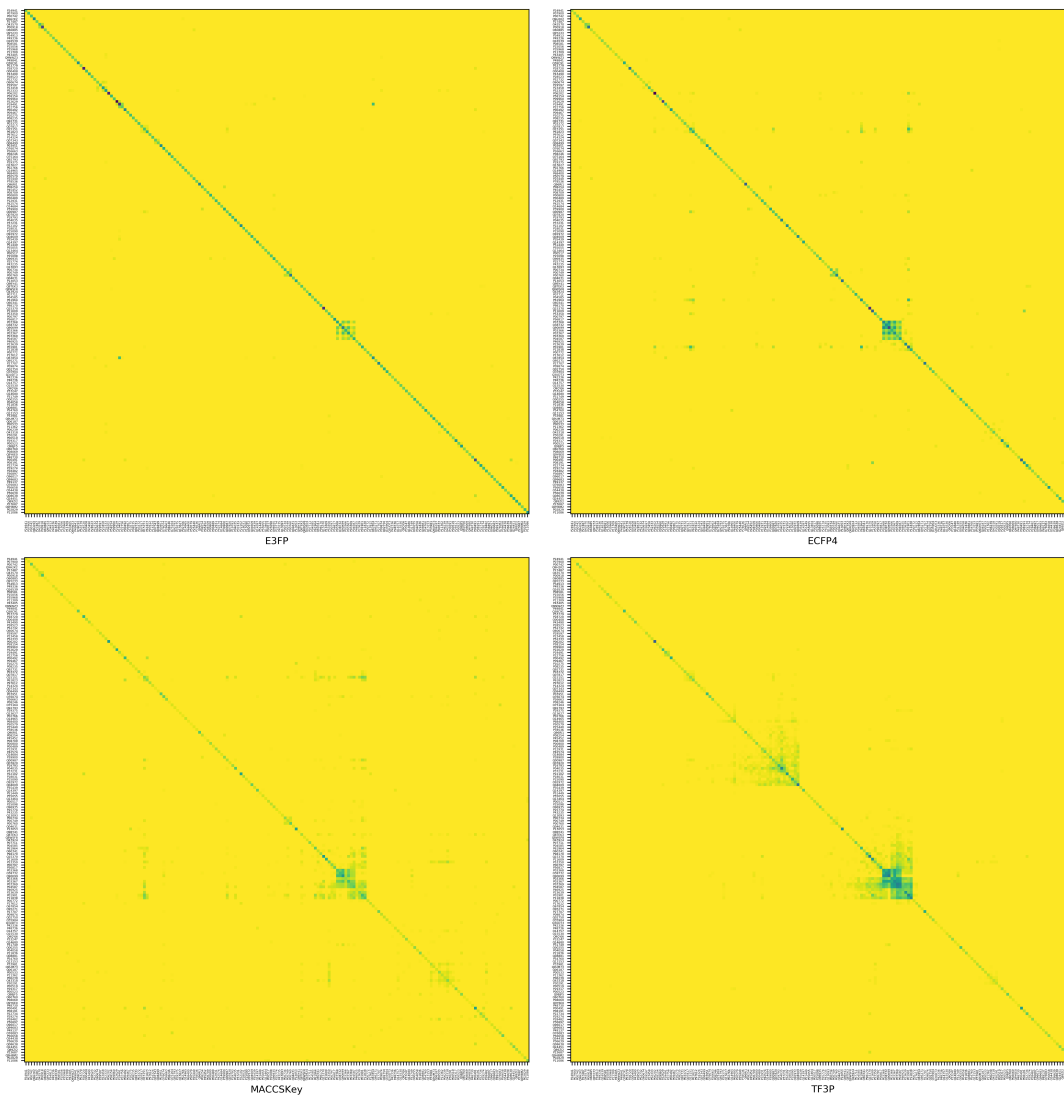


**Figure S3.** Heatmap of E-value of indicated targets calculated by SEA with four fingerprints. For high-resolution images, see <https://github.com/canisw/tf3p/tree/master/images>.

**Table S1.** RMSD vs. similarity by TF3P, E3FP and 2D FPs.

No. of Rotatable Bonds	RMSD ( $\text{\AA}$ , mean $\pm$ std)	Similarity by TF3P	Similarity by E3FP	Similarity by 2D FPs
0	$0.99 \pm 0.67$	$0.94 \pm 0.04$	$0.48 \pm 0.20$	$1.00 \pm 0.00$
1	$1.33 \pm 0.67$	$0.93 \pm 0.04$	$0.43 \pm 0.14$	$1.00 \pm 0.00$
2	$1.58 \pm 0.67$	$0.92 \pm 0.04$	$0.40 \pm 0.12$	$1.00 \pm 0.00$
3	$1.79 \pm 0.65$	$0.91 \pm 0.04$	$0.37 \pm 0.10$	$1.00 \pm 0.00$
4	$1.93 \pm 0.65$	$0.89 \pm 0.05$	$0.36 \pm 0.09$	$1.00 \pm 0.00$
5	$2.10 \pm 0.63$	$0.88 \pm 0.05$	$0.34 \pm 0.08$	$1.00 \pm 0.00$
6	$2.21 \pm 0.63$	$0.88 \pm 0.04$	$0.33 \pm 0.07$	$1.00 \pm 0.00$
7	$2.33 \pm 0.63$	$0.87 \pm 0.04$	$0.31 \pm 0.07$	$1.00 \pm 0.00$
8	$2.46 \pm 0.66$	$0.86 \pm 0.04$	$0.30 \pm 0.06$	$1.00 \pm 0.00$
9	$2.55 \pm 0.65$	$0.86 \pm 0.04$	$0.29 \pm 0.06$	$1.00 \pm 0.00$
10	$2.65 \pm 0.65$	$0.86 \pm 0.04$	$0.28 \pm 0.05$	$1.00 \pm 0.00$
11	$2.75 \pm 0.69$	$0.86 \pm 0.04$	$0.27 \pm 0.05$	$1.00 \pm 0.00$
12	$2.89 \pm 0.70$	$0.85 \pm 0.04$	$0.26 \pm 0.05$	$1.00 \pm 0.00$
13	$2.99 \pm 0.72$	$0.85 \pm 0.04$	$0.25 \pm 0.04$	$1.00 \pm 0.00$
14	$3.10 \pm 0.75$	$0.85 \pm 0.04$	$0.25 \pm 0.04$	$1.00 \pm 0.00$
15	$3.16 \pm 0.76$	$0.85 \pm 0.04$	$0.24 \pm 0.04$	$1.00 \pm 0.00$

**Table S2.** Kendall’s tau of FuzCav similarity vs. different fingerprints similarity for all active pairs from PDDBind v2018 General Set.

Top % <sup>a</sup>	TF3P	E3FP	MACCSKey	ECFP4
0.5	<b>0.22*</b>	0.11	0.12	0.12
1	<b>0.13*</b>	0.08	0.08	0.08
5	-0.01	<b>0.05*</b>	0.01	0.02
10	-0.02	<b>0.05*</b>	0.00	0.01
20	-0.02	<b>0.05*</b>	0.01	0.01
50	-0.00	<b>0.05*</b>	0.02	0.01
100	0.03	<b>0.05*</b>	<b>0.05*</b>	0.03

<sup>a</sup>: Sorted by the indicated fingerprint similarity.